RSC Advances

PAPER

View Article Online
View Journal | View Issue

Cite this: *RSC Adv.*, 2023, **13**, 1185

Stabile fluoro-benzene-based spacer for lead-free Dion–Jacobson perovskites†

Chih Shan Tan

Received 2nd December 2022
Accepted 15th December 2022

DOI: 10.1039/d2ra07675f

rsc.li/rsc-advances

Two-dimensional perovskite materials have been investigated as potential candidates for next-generation-wide band gap devices and lead-based perovskites are the most common materials within two-and three-dimensional structures due to their superior optoelectronic properties. Nevertheless, the stability and toxic element issues are the two significant shortcomings of device commercialization. The fluoro-benzene-based divalent ammonium spacer cations and replacing Zn^{2+} with Pb^{2+} will improve the two-dimensional perovskite stability. These stable lead-free wide band gap two-dimensional structures have better carrier mobility at high-temperature regions. Therefore, lead-free two-dimensional perovskites might be suitable for higher temperatures optoelectronic applications.

Introduction

Two-dimensional inorganic materials, such as hBN, MoS_2, BP, graphene, and TaS_2, are widely discovered for their unusual optoelectronic properties due to their unique layered structures within van der Waals gaps in device applications.[1–3] The two-dimensional inorganic materials usually grow by the metal–organic chemical vapor deposition (MOCVD) method, and it is hard to get a uniform thin film within a large area.[4,5] The comprehensive research on two-dimensional materials has extended toward organic–inorganic hybrid semiconductors, and it might be easy to fabricate a uniform thin film in a large area by spin coating or blading. Recently, two-dimensional organic–inorganic halide perovskites (OIHPs) have been investigated in the types of Ruddlesden–Popper (RP) and Dion–Jacobson (DJ) structures.[6–9] For the RP OIHPs, the organic ammonium cation spacer separates the perovskite structure and forms van der Waals gaps between the spacers. For the DJ OIHPs, the organic cation spacer separates the layered perovskite and connects the two layers by two diammonium cations. As a result, there is a van der Waals gap difference between RP and DJ OIHPs,[9] and the DJ OIHPs, without the van der Waals gaps, have better structural stability by avoiding the layer slide issue.

The van der Waals gap within the RP OIHPs makes it easy for the layers to slide, and might cause the phase to be unstable. Also, the structure is hard for the electrons and holes to move and worsen the optoelectronic properties.[7] Therefore, the DJ OIHPs without the van der Waals gap might be suitable for optoelectronic device applications, and there has been much research discussion on the DJ OIHPs.[10–16] The DJ OIHPs have opened a new extension research field with better stability and optoelectronic properties for the two-dimensional lead perovskites and are more complicated than the typical perovskite with the ABX_3 structure. The divalent ammonium spacer cations have different aromatic rings and functional groups between the two ammonium cations on the head and tail. The cation spacer, with the π electron, will improve the DJ OIHP structure stability, and the variation of the π electron condition might influence the two-dimensional crystal stability. Thus, the structure of divalent ammonium spacer cations needs further investigation. In this study, the different forms of the benzene rings and functional groups for the divalent ammonium spacer cations of the DJ OIHPs are screened using density functional theory (DFT) calculations.

The origin setup is to find directions for improving the structural stability and optoelectronic properties by changing the length and types of functional groups of the divalent ammonium spacer cations. By the phonon density of state calculation, the [4-(azaniumylmethyl)phenyl]methanaminium PbI_4 has better dynamic stability than benzene-1,4-bis(aminium) PbI_4 and 2-[4-(2-azaniumylethyl)phenyl]ethan-1-aminium PbI_4. Here, a suitable length of the divalent ammonium spacer cations was found. With different halides and methyl added to the benzene of the [4-(azaniumylmethyl)phenyl]methanaminium PbI_4, the [4-(azaniumylmethyl)-2-fluorophenyl]methanaminium PbI_4 and the [4-(azaniumylmethyl)-2,6-difluorophenyl]methanaminium PbI_4 have better dynamic stability. This indicates that the fluoro group could stabilize the DJ OIHPs in the divalent ammonium spacer cations. Finally, the Mg^{2+}, Ca^{2+}, Sr^{2+}, Zn^{2+}, Eu^{2+}, and Yb^{2+} are used to replace the Pb^{2+} cation of the [4-(azaniumylmethyl)-2-fluorophenyl]methanaminium PbI_4 and the [4-

Institute of Electronics, National Yang Ming Chiao Tung University, Hsinchu 30010, Taiwan. E-mail: cstan@nycu.edu.tw

† Electronic supplementary information (ESI) available: Additional symmetric crystal structure, the density of states, phonon dispersion, and detailed crystal information of Si (111) layers. See DOI: https://doi.org/10.1039/d2ra07675f

(azaniumylmethyl)-2,6-difluorophenyl]methanaminium PbI_4. The phonon calculation results showed that Zn^{2+} could be a candidate to form lead-free DJ OIHPs with better structural dynamic stability.

Results and discussion

Fig. 1a illustrates the DJ OIHP structure. The green and blue areas are the perovskites and the spacer parts. The blue squares at the two ends of the spacer are the ammonium cations, and the ammonium cations inserted at the A site of ABX_3 perovskite structure and transform the formula toward spacer cation-BX_4 perovskite (B = Pb and X = halides). Benzene has three pairs of π electrons, and the ability to move and oscillate π electrons will cause benzene to apply in conductive polymers[9] and semiconductors. Thus, the cation spacers with the benzene structure should be investigated for splitting the 3D perovskite structure toward the stable 2D perovskite. For the DJ OIHP solar cell, the poly(2,5-dimethylaniline) (PDMA) could be used as the divalent ammonium spacer cations with a 15.6% power conversion efficiency (PCE).[7]

Due to the high PCE of PDMA-based 2D solar cells, the PDMA-related divalent ammonium spacer cations within the DJ OIHP should be discussed. The PDMA is the benzene connected to two methyls symmetrically, and for both methyls, one of the hydrogens is changed to the NH_3^+. Indeed, the IUPAC (International Union of Pure and Applied Chemistry) name of PDMA is [4-(azaniumylmethyl)phenyl]methanaminium, and in this paper, the IUPAC name is preferred. The right spacer length of stable DJ OIHP needs to be found. In Fig. 1b, the benzene-1,4-bis(aminium), [4-(azaniumylmethyl)phenyl]methanaminium, and 2-[4-(2-azaniumylethyl)phenyl]ethan-1-aminium were created for discussion. The three divalent ammonium spacer cations were used to build the PbI_4-based DJ OIHPs for phonon density of the state (DOS) calculations. The imaginary part of the phonon DOS results of the three divalent ammonium spacer cations is shown in Table 1. For the imaginary part of phonon DOS, the lower portion usually means that the structure has better dynamic stability.[17–20] The imaginary (negative) phonon DOSs offer the phonon transition possibility from normal positive energy states to negative energy states, which will automatically lose bond energy. The more imaginary part of the phonon DOS accompanies more opportunities to lose bond energy by phonon and finally break the crystal structure. In Table 1, the [4-(azaniumylmethyl)phenyl]methanaminium PbI_4 has the lowest imaginary part of phonon DOS of 2.76%, than benzene-1,4-bis(aminium) PbI_4 of 6.55%, and 2-[4-(2-azaniumylethyl)phenyl]ethan-1-aminium PbI_4 of 2.81%, which means that the [4-(azaniumylmethyl)phenyl]methanaminium PbI_4 has better dynamic stability. According to the phonon calculation, the result helps to realize the reason that the PDMA-based DJ OIHP could be used for a solar cell with better device stability.[7]

Table 1 The imaginary part of the phonon DOS of benzene-1,4-bis(aminium) PbI_4, [4-(azaniumylmethyl)phenyl]methanaminium PbI_4, and 2-[4-(2-azaniumylethyl)phenyl]ethan-1-aminium PbI_4

Crystal structure	Imaginary part of phonon DOS (%)
Benzene-1,4-bis(aminium) PbI_4	6.55
[4-(Azaniumylmethyl)phenyl]methanaminium PbI_4	2.76
2-[4-(2-Azaniumylethyl)phenyl]ethan-1-aminium PbI_4	2.81

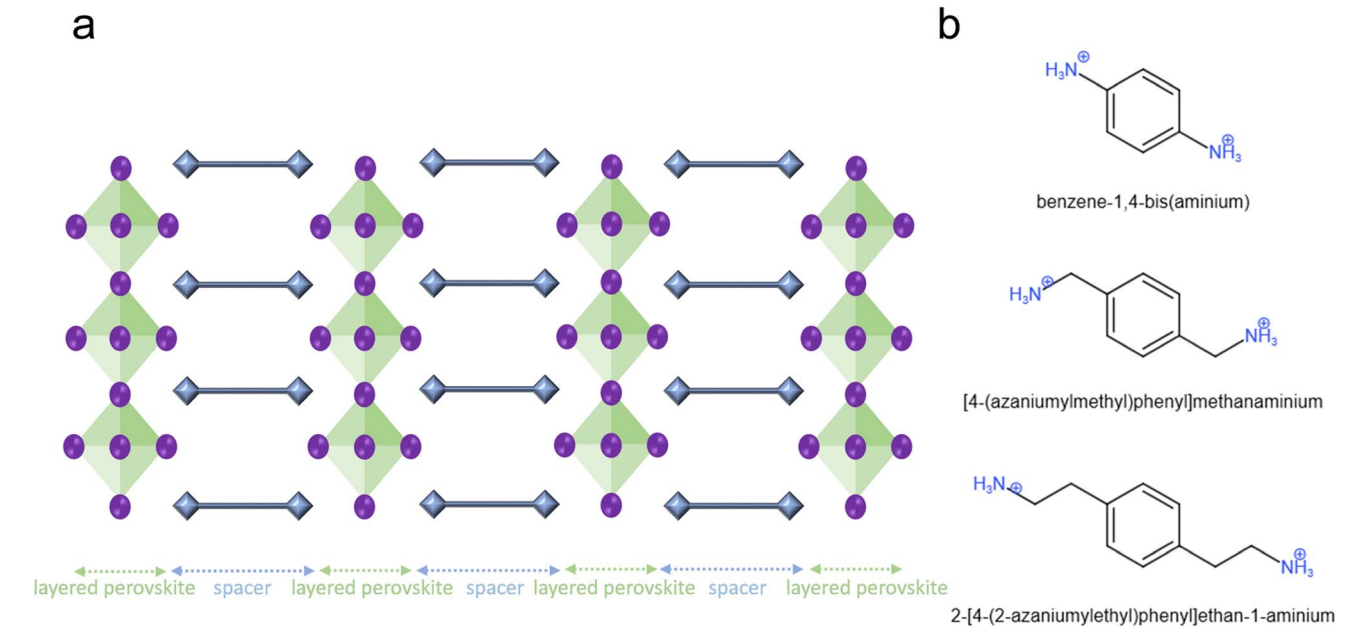

Fig. 1 The two-dimensional Dion–Jacobson perovskite and different spacer cations. (a) The 2D DJ layer structures are composed of a diammonium organic spacer layer (blue) and a 2D metal halide perovskite layer. (b) The typical two-diammonium aromatic spacer cations.

In Fig. S1 to S5,† the fluoro- (Fig. S1†), chloro- (Fig. S2†), bromo- (Fig. S3†), iodo- (Fig. S4†), and methyl (Fig. S5†) functional groups are added to the benzene circle by replacing the hydron or hydrons of the [4-(azaniumylmethyl)phenyl]methanaminium. For each functional group on the benzene of the [4-(azaniumylmethyl)phenyl]methanaminium structure, the variations are 2, 2-3, 2-5, 2-6, 2-3-6, and 2-3-5-6 sites. After a slight change in the functional groups of [4-(azaniumylmethyl)phenyl] methanaminium, the new divalent ammonium spacer cations are used to form the DJ OIHPs with layered PbI_4 for the phonon calculations. The related imaginary phonon DOSs are listed in Tables S1 to S5† for the dynamic stability discussion. Fig. S1 and Table S1† show that the fluoro-benzene-based spacer DJ OIHP variations have imaginary phonon DOS values from 0.69% to 2.89%. According to Fig. S2 and Table S2,† the chloro-benzene-based spacer DJ OIHP variations have imaginary phonon DOS values from 1.31% to 4.03%. In Fig. S3 and Table S3,† the bromo-benzene-based spacer DJ OIHP variations have imaginary phonon DOS values from 1.22% to 3.18%. In Fig. S4 and Table S4,† the iodo-benzene-based spacer DJ OIHP variations have imaginary phonon DOS values from 1.30% to 2.88%. In Fig. S5 and Table S5,† the methyl-benzene-based spacer DJ OIHP variations have imaginary phonon DOS values from 1.81% to 3.64%. The details of the methyl-benzene-based spacer DJ OIHPs shown in Fig. S5 and Table S5† have higher imaginary phonon DOS values, this point out that the methyl-benzene-based spacer DJ OIHPs might not be stable. The data also point out that the fluoro-benzene-based spacer DJ OIHPs have the lowest imaginary phonon DOSs of 0.69% and 0.71% for the [4-(azaniumylmethyl)-2,6-difluorophenyl]methanaminium PbI_4 and the [4-(azaniumylmethyl)-2-fluorophenyl]methanaminium PbI_4. These two DJ OIHPs are the only two structures, with Pb^{2+}, with imaginary phonon DOS values lower than 1% in this research.

The [4-(azaniumylmethyl)-2,6-difluorophenyl] methanaminium PbI_4 and the [4-(azaniumylmethyl)-2-fluorophenyl]methanaminium PbI_4 are *para*-divalent ammoniums. The *meta*-divalent ammoniums of the DJ OIHPs are built up for geometry stability discussion. Due to the divalent ammonium cations needed to link the layered PbI_4, in this research *ortho*-divalent ammonium was not used as the spacer. In Fig. S6,† the [3-(azaniumylmethyl)phenyl]methanaminium PbI_4 was used for the fluoro-benzene-based DJ OIHP discussion with the *para*-divalent ammoniums. There are ten positions for the fluoro to substitute on the benzene, and the calculated imaginary phonon DOSs are listed in Table S6.† In Table S6,† the [3-(azaniumylmethyl)phenyl]methanaminium PbI_4, *meta*-divalent ammoniums, have an imaginary phonon DOS of 1.44%, which is lower than the [4-(azaniumylmethyl)phenyl] methanaminium PbI_4, *para* divalent ammoniums, with imaginary phonon DOS of 2.76%, as shown in Table 1. Therefore, the *meta*-divalent ammoniums have better dynamic stabilities for

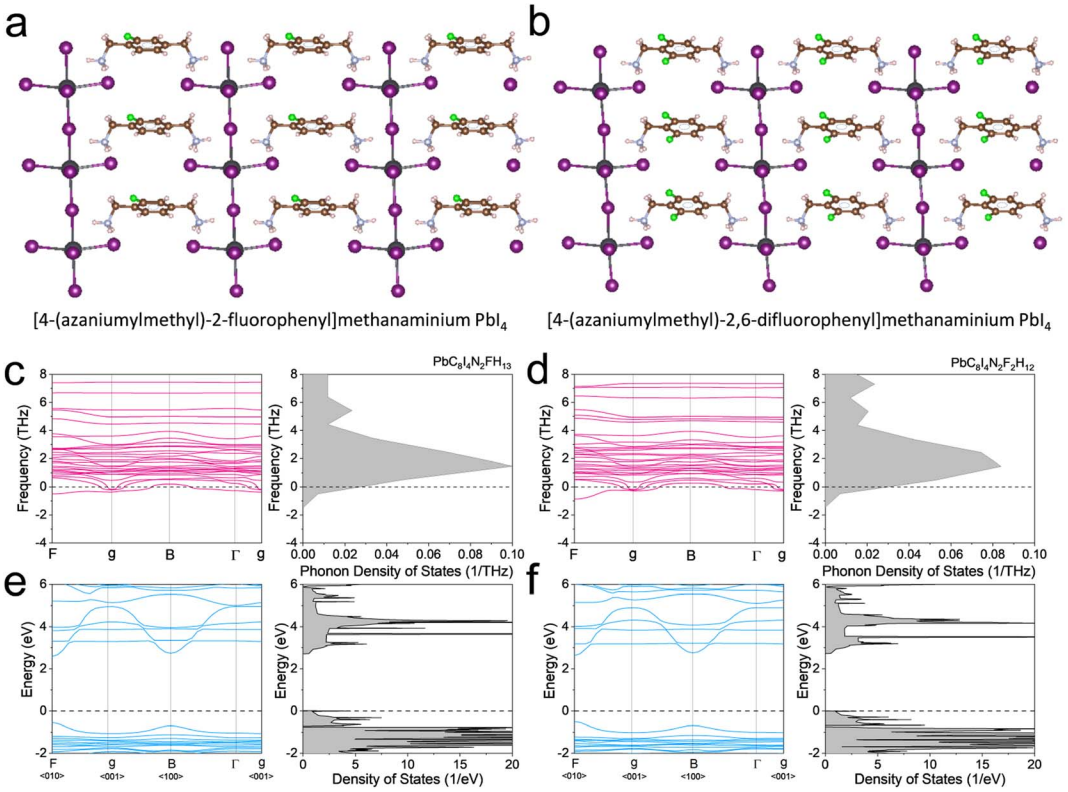

Fig. 2 The crystal structure, phonon band diagrams, and electron band diagrams of [4-(azaniumylmethyl)-2-fluorophenyl] methanaminium PbI_4 and [4-(azaniumylmethyl)-2,6-difluorophenyl] methanaminium PbI_4. (a and b) The crystal structures (c and d) The phonon band diagrams. (e and f) The electron band diagrams.

DJ OIHPs than the *para*, and the fluoro-based *meta*-divalent ammonium spacer should be discussed for further stability improvement. In Table S6,† the imaginary phonon DOS values are 1.44% to 3.35%, which means that the fluoro-based *para*-divalent ammonium spacer DJ OIHPs have the lower imaginary phonon DOS in Table S1.†

The structures of the [4-(azaniumylmethyl)-2-fluorophenyl] methanaminium PbI_4 and the [4-(azaniumylmethyl)-2,6-difluorophenyl]methanaminium PbI_4 are shown in Fig. 2a and b. For the [4-(azaniumylmethyl)-2-fluorophenyl]methanaminium PbI_4, the calculated phonon dispersion and phonon DOS diagrams are shown in Fig. 2c, and there are a few states below the zero dash line. The calculated phonon dispersion and phonon DOS diagrams are shown in Fig. 2d for the [4-(azaniumylmethyl)-2,6-difluorophenyl]methanaminium PbI_4, and few states are under zero. The band structure and electron DOS diagrams of the [4-(azaniumylmethyl)-2-fluorophenyl] methanaminium PbI_4 and [4-(azaniumylmethyl)-2,6-difluorophenyl]methanaminium PbI_4 are shown in Fig. 2e and f. Both of them have the same indirect band gaps of 2.72 eV. The two structures have one fluoro difference in benzene within the spacer, as shown in Fig. 2a and b. The phonon band diagrams differ slightly, as shown in Fig. 2c and d, but the electron band diagrams have no variation, as shown in Fig. 2e and f. The calculated XRD of the [4-(azaniumylmethyl)-2-fluorophenyl] methanaminium PbI_4 and [4-(azaniumylmethyl)-2,6-difluorophenyl]methanaminium PbI_4 are shown in Fig. 3a and b. These XRD patterns are nearly identical and could offer a reference for future experimental analysis. As the wavelength of the electron (0.025 Å) is shorter than that of the X-ray (1.54 Å), the electron diffraction patterns, with [001] zone axis, of the two DJ OIHPs were calculated and shown in Fig. 3c and d. The one fluoro difference is also hard to find in the electron diffraction patterns.

Although the flouro added on benzene could stabilize the DJ OIHP, the lead cation inside the DJ OIHP still had an environmental issue. The lead-free DJ OIHP should be an ideal two-dimensional material for future commercialized devices. Here, the Mg^{2+}, Ca^{2+}, Sr^{2+}, Zn^{2+}, Eu^{2+}, and Yb^{2+} cations are used to replace the Pb^{2+} cations in the [4-(azaniumylmethyl)-2-fluorophenyl]methanaminium PbI_4 and [4-(azaniumylmethyl)-2,6-difluorophenyl]methanaminium PbI_4, for the dynamic stability and optoelectronic property calculations. Table 4 lists the calculated results of lead-free DJ OIHPs, with the imaginary part of phonon DOS, the Debye temperature, and the band gap data. For the [4-(azaniumylmethyl)-2-fluorophenyl] methanaminium PbI_4 structure, Mg^{2+}, Sr^{2+}, Zn^{2+}, and Yb^{2+} replacement of Pb^{2+} could decrease the imaginary part of phonon DOS from 0.71% to 0.33%, 0.25%, 0.09%, and 0.31%, respectively. Mg^{2+} and Yb^{2+} are the two cations that could obtain a direct band gap during the replacement. For the [4-(azaniumylmethyl)-2,6-difluorophenyl]methanaminium PbI_4, the Mg^{2+}, Zn^{2+}, Eu^{2+}, and Yb^{2+} replacements of Pb^{2+} could decrease the imaginary part of the phonon DOS from 0.69% to 0.35%, 0.04%, 0.21%, and 0.48%, respectively. Mg^{2+} and Eu^{2+} are the two cations that can provide direct band gaps during the replacement. The Mg^{2+} cation replacement of Pb^{2+} could

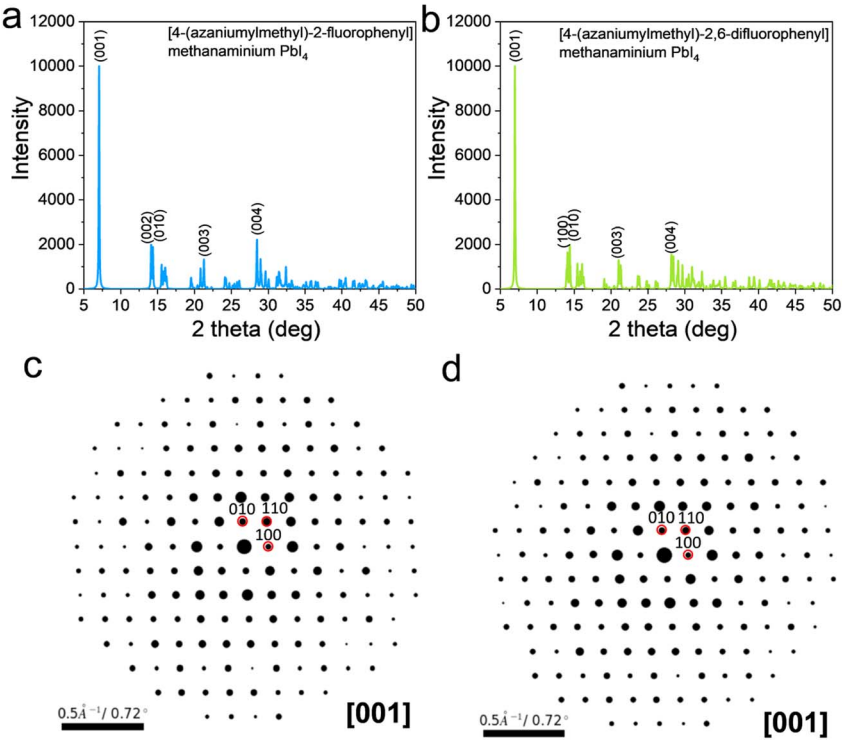

Fig. 3 The X-ray and electron diffraction patterns of [4-(azaniumylmethyl)-2-fluorophenyl] methanaminium PbI_4 and [4-(azaniumylmethyl)-2,6-difluorophenyl] methanaminium PbI_4. (a and b) The X-ray diffraction patterns (λ = 1.54 Å) (c and d) The electron diffraction patterns (λ = 0.025 Å).

change the band gap from the indirect band gap to direct in DJ OIHP. The Mg^{2+}, Zn^{2+}, and Yb^{2+} replacements of Pb^2 could improve the dynamic stability in DJ OIHP. The [4-(azaniumylmethyl)-2-fluorophenyl]methanaminium ZnI_4 and [4-(azaniumylmethyl)-2,6-difluorophenyl]methanaminium ZnI_4 are the dynamic stable structures with the ultra-low imaginary part of the phonon DOS of 0.09% and 0.04%, and indirect band gaps as 4.00 eV and 3.81 eV, respectively. Even increasing the k point setting from $4 \times 5 \times 3$ to $7 \times 7 \times 4$, the imaginary part of the phonon DOS of [4-(azaniumylmethyl)-2-fluorophenyl] methanaminium ZnI_4 and [4-(azaniumylmethyl)-2,6-difluorophenyl]methanaminium ZnI_4 increased to 1.55% and 1.39%, respectively, remaining in lower amounts.

The properties of the lead-free DJ OIHPs should be thoroughly discussed for further application, such as carrier mobility, shown in Fig. 4a and b, electrical conductivity shown in Fig. 4c and d, and carrier density shown in Fig. 4e and f. Fig. 4a and b show that the Pb^{2+} cations inside the DJ OIHPs have the highest values for temperature-dependent carrier mobility. For the temperature-dependent electrical conductivity shown in Fig. 4c and d, the Pb^{2+} cations inside the DJ OIHPs have the highest values. In Fig. 4e, only the [4-(azaniumylmethyl)-2-fluorophenyl]methanaminium MgI_4 is an n-type semiconductor with a positive value, and the others are p-type semiconductors. In Fig. 4f, only the [4-(azaniumylmethyl)-2,6-difluorophenyl]methanaminium MgI_4

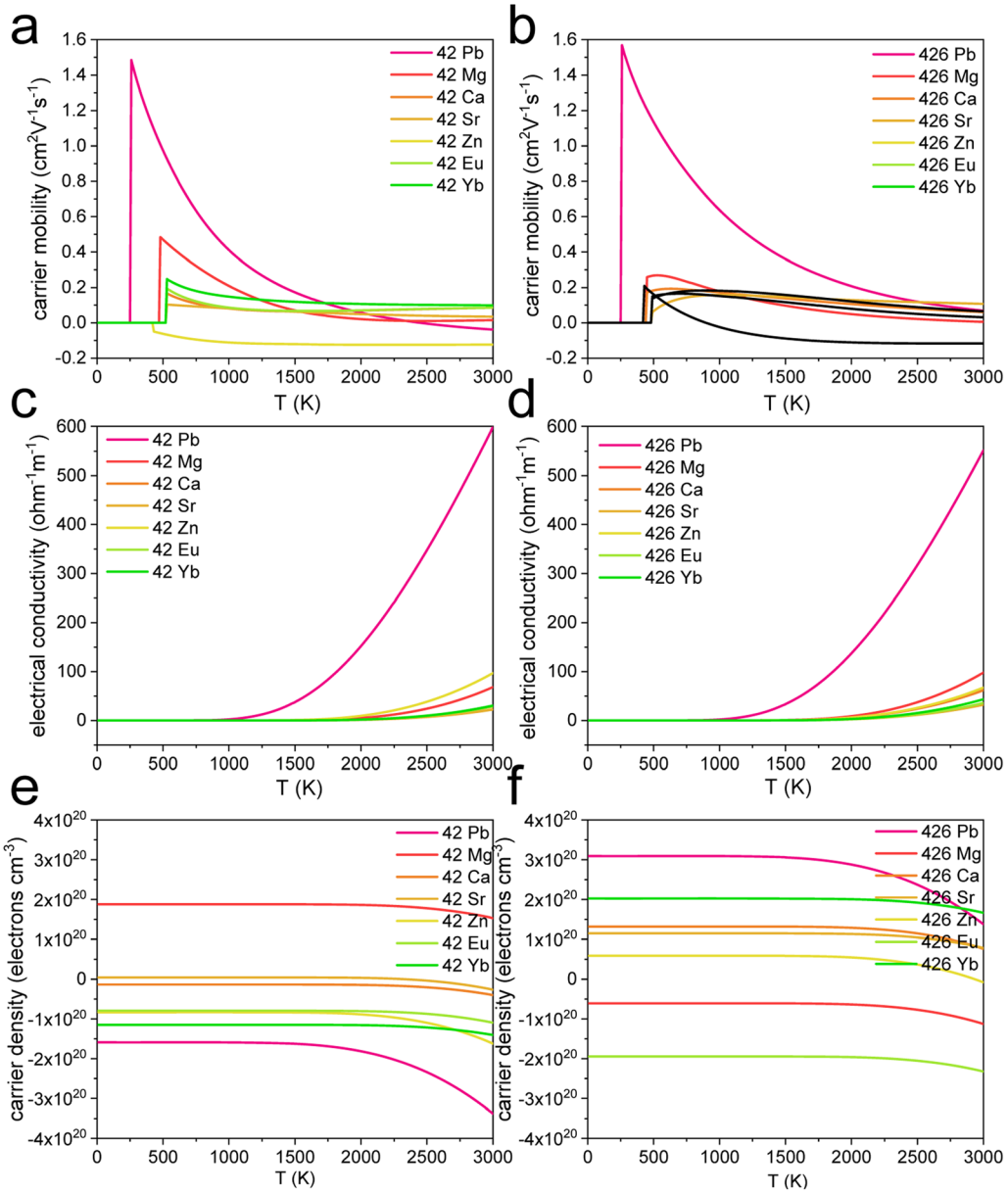

Fig. 4 The carrier mobility, electrical conductivity, and carrier density of [4-(azaniumylmethyl)-2-fluorophenyl] methanaminium XI_4 and [4-(azaniumylmethyl)-2,6-difluorophenyl] methanaminium XI_4. (X = Pb, Mg, Ca, Sr, Zn, Eu, and Yb) (a and b) The carrier mobilities. (c and d) The electrical conductivities. (e and f) The carrier densities.

Table 2 The imaginary part of phonon DOS, Debye temperature, and band gap of [4-(azaniumylmethyl)-2-fluorophenyl] methanaminium XI_4 and [4-(azaniumylmethyl)-2,6-difluorophenyl] methanaminium XI_4. (X = Pb, Mg, Ca, Sr, Zn, Eu, and Yb)

[4-(Azaniumylmethyl)-2-fluorophenyl] methanaminium XI_4	Imaginary part of phonon DOS (%)	Debye temperature (θ_D) (K)	Band gap (eV)	[4-(Azaniumylmethyl)-2,6-difluorophenyl]methanaminium XI_4	Imaginary part of phonon DOS (%)	Debye temperature (θ_D) (K)	Band gap (eV)
X = Pb	0.71	101	2.72 (indirect)	X = Pb	0.69	94	2.72 (indirect)
X = Mg	0.33	116	4.03 (direct)	X = Mg	0.35	107	3.80 (direct)
X = Ca	0.90	103	4.36 (indirect)	X = Ca	1.17	103	4.02 (indirect)
X = Sr	0.25	97	4.47 (indirect)	X = Sr	3.67	114	4.08 (indirect)
X = Zn	0.09	108	4.00 (indirect)	X = Zn	0.04	111	3.81 (indirect)
X = Eu	0.90	102	4.44 (indirect)	X = Eu	0.21	105	4.09 (direct)
X = Yb	0.31	105	4.36 (direct)	X = Yb	0.48	104	4.03 (indirect)

Table 3 The electrical conductivity and carrier mobility of [4-(azaniumylmethyl)-2-fluorophenyl] methanaminium XI_4. (X = Pb, Mg, Ca, Sr, Zn, Eu, and Yb) (σ (ohm^{-1} m^{-1}) is electrical conductivity and μ (cm^2 V^{-1} s^{-1}) is the carrier mobility.)

[4-(Azaniumylmethyl)-2-fluorophenyl] methanaminium XI_4	X = Pb		X = Mg		X = Ca		X = Sr		X = Zn		X = Eu		X = Yb	
	σ	μ	σ	μ	σ	μ	σ	μ	σ	μ	σ	μ	σ	μ
300 K	1.64×10^{-8}	1.37	0	0	0	0	0	0	0	0	0	0	0	0
350 K	7.05×10^{-7}	1.26	0	0	0	0	0	0	0	0	0	0	0	0
400 K	1.20×10^{-5}	1.15	-2.56×10^{-33}	0	0	0	0	0	0	0	0	0	0	0
450 K	1.10×10^{-4}	1.06	-2.30×10^{-31}	0	-4.78×10^{-33}	0	-3.06×10^{-33}	0	2.37×10^{-10}	−0.05	-5.96×10^{-33}	0	-5.46×10^{-33}	0
500 K	6.53×10^{-4}	0.97	3.44×10^{-10}	0.47	-2.56×10^{-31}	0	-1.71×10^{-31}	0	5.44×10^{-9}	−0.06	-3.01×10^{-31}	0	-2.87×10^{-31}	0
550 K	2.83×10^{-3}	0.90	5.67×10^{-9}	0.44	2.80×10^{-10}	0.16	1.90×10^{-10}	0.10	7.07×10^{-8}	−0.07	3.23×10^{-10}	0.18	3.11×10^{-10}	0.24
600 K	9.63×10^{-3}	0.82	5.89×10^{-8}	0.41	3.72×10^{-9}	0.14	2.55×10^{-9}	0.10	6.02×10^{-7}	−0.08	4.25×10^{-9}	0.16	4.13×10^{-9}	0.22

Table 4 The electrical conductivity and carrier mobility of [4-(azaniumylmethyl)-2,6-difluorophenyl]methanaminium XI_4. (X = Pb, Mg, Ca, Sr, Zn, Eu, and Yb) (σ (ohm^{-1} m^{-1}) is electrical conductivity and μ (cm^2 V^{-1} s^{-1}) is carrier mobility.)

[4-(Azaniumylmethyl)-2,6-difluorophenyl]methanaminium	X = Pb		X = Mg		X = Ca		X = Sr		X = Zn		X = Eu		X = Yb	
XI_4	σ	μ	σ	μ	σ	μ	σ	μ	σ	μ	σ	μ	σ	μ
300 K	1.01×10^{-8}	1.47	0	0	0	0	0	0	0	0	0	0	0	0
350 K	4.64×10^{-7}	1.37	-2.77×10^{-35}	0	-1.27×10^{-35}	0	0	0	-1.58×10^{-34}	0	0	0	0	0
400 K	8.33×10^{-6}	1.28	-5.53×10^{-32}	0	-4.77×10^{-32}	0	-1.23×10^{-33}	0	-6.53×10^{-32}	0	-1.30×10^{-33}	0	-1.27×10^{-33}	0
450 K	7.96×10^{-5}	1.21	1.41×10^{-10}	0.26	1.21×10^{-10}	0.17	-1.25×10^{-31}	0	1.54×10^{-10}	0.19	-1.28×10^{-31}	0	-1.31×10^{-31}	0
500 K	4.88×10^{-4}	1.14	3.33×10^{-9}	0.27	2.84×10^{-9}	0.18	1.92×10^{-10}	0.07	3.44×10^{-9}	0.16	1.96×10^{-10}	0.14	2.04×10^{-10}	0.15
550 K	2.17×10^{-3}	1.07	4.44×10^{-8}	0.27	3.77×10^{-8}	0.19	3.2×10^{-9}	0.09	4.37×10^{-8}	0.13	3.29×10^{-9}	0.15	3.46×10^{-9}	0.16
600 K	7.56×10^{-3}	1.01	3.86×10^{-7}	0.26	3.25×10^{-7}	0.19	3.36×10^{-8}	0.11	3.66×10^{-7}	0.11	3.44×10^{-8}	0.16	3.67×10^{-8}	0.16

and [4-(azaniumylmethyl)-2,6-difluorophenyl]methanaminium EuI_4 are p-type semiconductors, with the negative values, and the others are n-type semiconductors. The exact value of the carrier mobility and electrical conductivity for [4-(azaniumylmethyl)-2-fluorophenyl]methanaminium XI_4 and [4-(azaniumylmethyl)-2,6-difluorophenyl]methanaminium XI_4 are listed in Tables 3 and 4, respectively, and it was found that the lead-free DJ OIHPs became a semi-conductor at the higher temperature range. For the Zn-based lead-free DJ OIHPs, the working temperature should be higher than 450 K. As shown in Tables 3 and 4, the lead-containing DJ OIHPs have better optoelectronic properties than the lead-free ones and will be more suitable for device applications at room temperature. However, the lead-free DJ OIHPs have wider bands of 3.80 eV to 4.47 eV, as shown in Table 2, which is wider than the lead DJ OIHPs of 2.72 eV and are more stable. Therefore, the lead-free DJ OIHPs have the potential for wide-band gap device applications.

Conclusions

By the phonon calculation, the fluoro-benzene-based divalent ammonium spacer cations could stabilize the DJ OIHP with increased dynamic stability. The Mg^{2+}, Zn^{2+}, and Yb^{2+} replacements of Pb^{2+} could improve the dynamic stability of the lead DJ OIHPs. Here, the [4-(azaniumylmethyl)-2-fluorophenyl] methanaminium ZnI_4 (indirect, 4.00 eV) and [4-(azaniumylmethyl)-2,6-difluorophenyl]methanaminium ZnI_4 (indirect, 3.81 eV) are the dynamic stable DJ OIHPs and might exist naturally with the imaginary part of phonon DOS as 0.09% and 0.04%. In this study, it was found that the two stable Zn-based lead-free DJ OIHPs could be used in future high-temperature ultra-wide band gap optoelectronic applications. Here, the [4-(azaniumylmethyl)-2-fluorophenyl] methanaminium ZnI_4 (indirect, 4.00 eV) and [4-(azaniumylmethyl)-2,6-difluorophenyl]methanaminium ZnI_4 (indirect, 3.81 eV) are the dynamic stable DJ OIHPs and might exist naturally with the imaginary part of phonon DOS as 0.09% and 0.04%, respectively. In this research, it was found that the two stable Zn-based lead-free DJ OIHPs could be used in future high-temperature ultra-wide band gap optoelectronic applications. Here, the [4-(azaniumylmethyl)-2-fluorophenyl] methanaminium ZnI_4 (indirect, 4.00 eV) and [4-(azaniumylmethyl)-2,6-difluorophenyl]methanaminium ZnI_4 (indirect, 3.81 eV) are the dynamic stable DJ OIHPs and might exist naturally with the imaginary part of phonon DOS as 0.09% and 0.04%, respectively. In this research, it was found that the two stable Zn-based lead-free DJ OIHPs could be used in future high-temperature ultra-wide band gap optoelectronic applications. Here, the [4-(azaniumylmethyl)-2-fluorophenyl] methanaminium ZnI_4 (indirect, 4.00 eV) and [4-(azaniumylmethyl)-2,6-difluorophenyl]methanaminium ZnI_4 (indirect, 3.81 eV) are the dynamic stable DJ OIHPs and might exist naturally with the imaginary part of phonon DOS as 0.09% and 0.04%, respectively. In this research, it was found that two stable Zn-based lead-free DJ OIHPs could be used in future high-temperature ultra-wide band gap optoelectronic

applications. Here, the [4-(azaniumylmethyl)-2-fluorophenyl] methanaminium ZnI_4 (indirect, 4.00 eV) and [4-(azaniumylmethyl)-2,6-difluorophenyl]methanaminium ZnI_4 (indirect, 3.81 eV) are the dynamic stable DJ OIHPs and might exist naturally with the imaginary part of phonon DOS, as 0.09% and 0.04%, respectively. This research found that two stable Zn-based lead-free DJ OIHPs could be used in future high-temperature ultra-wide band gap optoelectronic applications. Here, the [4-(azaniumylmethyl)-2-fluorophenyl] methanaminium ZnI_4 (indirect, 4.00 eV) and [4-(azaniumylmethyl)-2,6-difluorophenyl]methanaminium ZnI_4 (indirect, 3.81 eV) are the dynamic stable DJ OIHPs and might exist naturally with the imaginary part of phonon DOS, as 0.09% and 0.04%, respectively. In this research, it was found that two stable Zn-based lead-free DJ OIHPs could be used in future high-temperature ultra-wide band gap optoelectronic applications. Here, the [4-(azaniumylmethyl)-2-fluorophenyl] methanaminium ZnI_4 (indirect, 4.00 eV) and [4-(azaniumylmethyl)-2,6-difluorophenyl]methanaminium ZnI_4 (indirect, 3.81 eV) are the dynamic stable DJ OIHPs and might exist naturally with the imaginary part of phonon DOS, as 0.09% and 0.04%, respectively. In this research, it was found that the two stable Zn-based lead-free DJ OIHPs could be used in future high-temperature ultra-wide band gap optoelectronic applications. Here, the [4-(azaniumylmethyl)-2-fluorophenyl] methanaminium ZnI_4 (indirect, 4.00 eV) and [4-(azaniumylmethyl)-2,6-difluorophenyl]methanaminium ZnI_4 (indirect, 3.81 eV) are the dynamic stable DJ OIHPs and might exist naturally with the imaginary part of phonon DOS, as 0.09% and 0.04%, respectively. In this research, it was found that two stable Zn-based lead-free DJ OIHPs could be used in future high-temperature ultra-wide band gap optoelectronic applications. Here, the [4-(azaniumylmethyl)-2-fluorophenyl] methanaminium ZnI_4 (indirect, 4.00 eV) and [4-(azaniumylmethyl)-2,6-difluorophenyl]methanaminium ZnI_4 (indirect, 3.81 eV) are the dynamic stable DJ OIHPs and might exist naturally with the imaginary part of phonon DOS, as 0.09% and 0.04%, respectively. In this research, it was found that the two stable Zn-based lead-free DJ OIHPs could be used in future high-temperature ultra-wide band gap optoelectronic applications.

Method

The calculations were processed using VASP (Vienna *ab initio* Simulation Package)[21–23] with different functionals for various applications. The new build-up structures were processed for structure optimization calculation using the GGA-PBEsol,[24] with a default plane-wave cutoff energy of 500 eV. The requested *k*-spacing was 0.3 per Angstrom, which led to a $4 \times 4 \times 2$ mesh, and using first-order Methfessel–Paxton smearing with a width of 0.2 eV. The phonon calculations were conducted using GGA-PBE,[25] with a plane-wave cutoff of 500 eV, *k*-spacing of $4 \times 5 \times 3$ and $7 \times 7 \times 4$ mesh, and a Methfessel–Paxton smearing width of 0.2 eV. The $4 \times 5 \times 3$ mesh was set for the first phonon state screen, and the $7 \times 7 \times 4$ mesh was set for the detail phonon state discussion. The semiconductor properties (electrical conductivity, carrier mobility, and carrier density) were calculated within Boltzmann's transport theory (BoltzTraP), processed by GGA-PBEsol, with the chemical potential set as 18 mu within 42 functions. The chemical potential setup used $MAPbCl_3$ as a reference structure, and 18 mu within 42 functions could obtain the calculation of electrical conductivity as 2.68×10^{-6} (ohm^{-1} m^{-1}) at room temperature, which is close to the experimental result of 2.7×10^{-6} (ohm^{-1} m^{-1}).[20] The Meta GGA-MBJLDA[26,27] was used for the band structure calculation with a plane-wave cutoff energy of 500 eV, *k*-spacing as $4 \times 4 \times 2$ mesh, and linear-tetrahedron method. The XRD and electron diffraction pattern calculations were performed using Mercury and PTLab software.

Author contributions

Chih Shan Tan initiated all the research ideas, performed calculations, and completed the paper writing independently.

Conflicts of interest

The authors declare no competing financial interest.

Acknowledgements

This work was funded by the Ministry of Science and Technology of Taiwan (Grants MOST 111-2636-E-A49-002).

References

1 L. Wang, I. Meric, P. Y. Huang, Q. Gao, Y. Gao, H. Tran, T. Taniguchi, K. Watanabe, L. M. Campos, D. A. Muller, J. Guo, P. Kim, J. Hone, K. L. Shepard and C. R. Dean, One-dimensional electrical contact to a two-dimensional material, *Science*, 2013, **342**, 614–617.

2 F. Xia, H. Wang, D. Xiao, M. Dubey and A. Ramasubramaniam, Two-dimensional material nanophotonics, *Nat. Photonics*, 2014, **8**, 899–907.

3 B. Shao, A. Eich, C. Sanders, A. S. Ngankeu, M. Bianchi, P. Hofmann, A. A. Khajetoorians and T. O. Wehling, Pseudodoping of a metallic two-dimensional material by the supporting substrate, *Nat. Commun.*, 2019, **10**, 180.

4 Y. Kim, S. S. Cruz, K. Lee, B. O. Alawode, C. Choi, Y. Song, J. M. Johnson, C. Heidelberger, W. Kong, S. Choi, K. Qiao, I. Almansouri, E. A. Fitzgerald, J. Kong, A. M. Kolpak, J. Hwang and J. Kim, Remote epitaxy through graphene enables two-dimensional material-based layer transfer, *Nature*, 2017, **544**, 340–343.

5 Y. Liu, Y. Huang and X. Duan, Van der Waals integration before and beyond two-dimensional materials, *Nature*, 2019, **567**, 323–333.

6 H. Tsai, W. Nie, J.-C. Blancon, C. C. Stoumpos, R. Asadpour, B. Harutyunyan, A. J. Neukirch, R. Verduzco, J. J. Crochet, S. Tretiak, L. Pedesseau, J. Even, M. A. Alam, G. Gupta, J. Lou, P. M. Ajayan, M. J. Bedzyk and M. G. Kanatzidis, High-efficiency two-dimensional Ruddlesden-Popper perovskite solar cells, *Nature*, 2016, **536**, 312–316.

7 P. Huang, S. Kazim, M. Wang and S. Ahmad, Toward Phase Stability: Dion–Jacobson Layered Perovskite for Solar Cells, *ACS Energy Lett.*, 2019, **4**, 2960–2974.
8 B.-E. Cohen, Y. Li, Q. Meng and L. Etgar, Dion-Jacobson Two-Dimensional Perovskite Solar Cells Based on Benzene Dimethanammonium Cation, *Nano Lett.*, 2019, **19**, 2588–2597.
9 D. Sirbu, F. H. Balogun, R. L. Milot and P. Docampo, Layered Perovskites in Solar Cells: Structure, Optoelectronic Properties, and Device Design, *Adv. Energy Mater.*, 2021, **11**, 2003877.
10 B.-E. Cohen, T. Binyamin, T. Ben-Tzvi, O. Goldberg, A. Schlesinger, I. Balberg, O. Millo, E. Gross, D. Azulay and L. Etgar, Hydroxyl Functional Groups in Two-Dimensional Dion–Jacobson Perovskite Solar Cells, *ACS Energy Lett.*, 2022, **7**, 217–225.
11 D. Wang, S.-C. Chen and Q. Zheng, Enhancing the efficiency and stability of two-dimensional Dion–Jacobson perovskite solar cells using a fluorinated diammonium spacer, *J. Mater. Chem. A*, 2021, **9**, 11778–11786.
12 Y. Liu, L. K. Ono, G. Tong, H. Zhang and Y. Qi, Two-Dimensional Dion–Jacobson Structure Perovskites for Efficient Sky-Blue Light-Emitting Diodes, *ACS Energy Lett.*, 2021, **6**, 908–914.
13 G. Lv, L. Li, D. Lu, Z. Xu, Y. Dong, Q. Li, Z. Chang, W.-J. Yin and Y. Liu, Multiple-Noncovalent-Interaction-Stabilized Layered Dion-Jacobson Perovskite for Efficient Solar Cells, *Nano Lett.*, 2021, **21**, 5788–5797.
14 H. Wu, X. Lian, J. Li, Y. Zhang, G. Zhou, X. Wen, Z. Xie, H. Zhu, G. Wu and H. Chen, Merged interface construction toward ultra-low Voc loss in inverted two-dimensional Dion–Jacobson perovskite solar cells with efficiency over 18%, *J. Mater. Chem. A*, 2021, **9**, 12566–12573.
15 Z. Xu, D. Lu, X. Dong, M. Chen, Q. Fu and Y. Liu, Highly Efficient and Stable Dion-Jacobson Perovskite Solar Cells Enabled by Extended π-Conjugation of Organic Spacer, *Adv. Mater.*, 2021, **33**, e2105083.
16 X. Zhang, T. Yang, X. Ren, L. Zhang, K. Zhao and S. Liu, Film Formation Control for High Performance Dion–Jacobson 2D Perovskite Solar Cells, *Adv. Energy Mater.*, 2021, **11**, 2002733.
17 C. S. Tan, Density Functional Theory Study of Metallic Silicon (111) Plane Structures, *ACS Omega*, 2022, **7**, 5385–5392.
18 C. S. Tan, Lead-Free Ultra-Wide Direct Bandgap Perovskite EACaI 3, *IEEE Trans. Nanotechnol.*, 2022, **21**, 66–70.
19 C. S. Tan, Transition Metal Ions in Methylammonium Chloride Perovskites, *ACS Omega*, 2022, **7**, 1412–1419.
20 C. S. Tan and C. C. Yang, Optoelectronic Properties Prediction of Lead-Free Methylammonium Alkaline-Earth Perovskite Based on DFT Calculations, *ACS Omega*, 2022, **7**, 16204–16210.
21 G. Kresse and J. Hafner, Ab initio molecular dynamics for liquid metals, *Phys. Rev. B: Condens. Matter Mater. Phys.*, 1993, **47**, 558–561.
22 G. Kresse and J. Furthmüller, Efficient iterative schemes for *ab initio* total-energy calculations using a plane-wave basis set, *Phys. Rev. B: Condens. Matter Mater. Phys.*, 1996, **54**, 11169–11186.
23 G. Kresse and J. Furthmüller, Efficiency of *ab initio* total energy calculations for metals and semiconductors using a plane-wave basis set, *Comput. Mater. Sci.*, 1996, **6**, 15–50.
24 G. I. Csonka, J. P. Perdew, A. Ruzsinszky, P. H. T. Philipsen, S. Lebègue, J. Paier, O. A. Vydrov and J. G. Ángyán, Assessing the performance of recent density functionals for bulk solids, *Phys. Rev. B: Condens. Matter Mater. Phys.*, 2009, **79**, 155107.
25 J. P. Perdew, K. Burke and M. Ernzerhof, Generalized Gradient Approximation Made Simple, *Phys. Rev. Lett.*, 1996, **77**, 3865; *Phys. Rev. Lett.*, 1997, **78**, 1396.
26 F. Tran and P. Blaha, Accurate band gaps of semiconductors and insulators with a semilocal exchange-correlation potential, *Phys. Rev. Lett.*, 2009, **102**, 226401.
27 A. D. Becke and E. R. Johnson, A simple effective potential for exchange, *J. Chem. Phys.*, 2006, **124**, 221101.